ABSTRACT

Remote Estimation of Aquatic Sediment Density in the Presence of Scatter

Adam E. Collard, M.S.

Chairman: John A. Dunbar, Ph.D.

The accuracy of an acoustic method is tested for its ability to estimate the density of the first few meters of shallow marine sediments. Normal incidence reflections from a 16 kHz omnidirectional source are collected using a single hydrophone directly above the source. An empirical relationship is then used to estimate the sediment density from the normal incidence reflections. Due to the high frequency source and centimeter scale inhomogeneities in the sediment, a considerable amount of noise or scatter is produced. The scattered energy is incoherent, and therefore removable through signal processing methods. These processing methods are tested for their effectiveness using synthetic data generated by a finite element model. Lastly, as a proof of concept, the processing methods are applied to acoustic data and core samples collected at Lake Lavon (Wylie, Texas).

Remote Estimation of Aquatic Sediment Density in the Presence of Scatter

by

Adam E. Collard, B.S.

A Thesis

Approved by the Department of Geology

_____

Stacy C. Atchley, Ph.D., Chairperson

Submitted to the Graduate Faculty of
Baylor University in Partial Fulfillment of the
Requirements for the Degree
of

Master of Science

Approved by the Thesis Committee

_____

John A. Dunbar, Ph.D., Chairperson

_____

Robert Jay Pulliam, Ph.D.

_____

Gregory A. Benesh, Ph.D.

Accepted by the Graduate School

December 2015

_____

J. Larry Lyon, Ph.D., Dean

Page bearing signatures is kept on file in the Graduate School.

TABLE OF CONTENTS

LIST OF FIGURES

LIST OF TABLES

ACKNOWLEDGMENTS

Foremost, I would like to thank my advisor, Dr. John A. Dunbar, who has seen this project through from data acquisition to my thesis. I would also like to thank Dr. Robert Jay Pulliam and Dr. Greg A. Benesh for their time and support. I would like to thank my family for their support throughout my entire academic career. A special thank you to my brother Corey who inspired me to pursue a graduate degree. Lastly, I would like to thank Frank Sepulveda for his mentorship.

CHAPTER ONE

Introduction

This study evaluates the accuracy and limitations of a novel acoustic method to estimate soft sediment density prior to dredging. These soft sediments are commonly navigable for vessels but appear on pre-dredging depth surveys as an unnavigable hard bottom. As a result, these sediments are dredged unnecessarily and at a great expense. Existing methods to alleviate the needless dredging of soft sediments are time consuming and cost prohibitive. This study evaluates a cost efficient method to evaluate sedimentary layers and aid dredging operations.

CHAPTER TWO

Manuscript One

Remote Estimation of Aquatic Sediment Density in the Presence of Scatter

1. Introduction

The US Army Corps of Engineers (USACE) spent $1.2 billion dredging 235 million cubic meters of material in 2012 [*Verna*, 2013]. Dredging is continuously performed to maintain navigable depths in canals, rivers, harbors and marinas. Fathometers are used in support of such dredging activities to measure the depth to the sedimentary water bottom to determine if navigable depths exist before and after dredging [*Luccio*, 2014]. Suspended sediment, known as fluid mud, appears as a solid bottom on fathometer surveys; however, these sediments do not impede vessel navigation [*McAnally et al.*, 2007] [*Hall*, 2014]. Because the fluid mud layer appears to be the solid bottom on fathometer records, many navigable areas are unnecessarily dredged [*Kamphuis et al.*, 2013]. During the dredging process the sedimentary layer is disturbed, which results in additional suspended sediment and a new fluid mud layer is created [*Smith and Friedrichs*, 2011]. This new fluid mud layer appears as the solid bottom again and depth surveys indicate that additional dredging is required. This dredging is very costly for marinas and harbors. Determining the material properties of the sediment to be dredged has traditionally been accomplished through direct sampling (i.e., coring or bottom grab sampling), and *in situ* measurements (i.e., drop cone tests) [*Welp*, 2010]

[*McAnally et al.*, 2007]. However, these methods are too expensive and time consuming to use over large areas.

Direct sampling in conjunction with lab measurements provide a wider range of bulk material properties than *in situ* measurements [*Jones*, 2001]. Coring is popular because it provides a clear distinction of sediment properties with depth. Cores are typically cataloged and taken to a lab where material properties can be determined using different methods [*Jones*, 2001] [*Blomqvist*, 1985].

Even though coring provides accurate measurements, there are several reasons why it is not the best solution for supporting dredging operations. Coring is costly and time consuming to sample, catalog, and perform measurements on samples. Coring samples are taken from point locations. The core's measured material properties are only applicable to the immediate area. As a result, spatial coverage is determined based on the number of samples. Increasing core sample density dramatically increases the survey time. For these reasons, coring does not provide a fast and cost effective solution for the survey of the large areas needed to support dredging operations. However, coring remains the standard for providing ground truth and direct measurement of sediment properties.

Acoustic bottom typing methods, as an alternative to coring, are used to interpret the characteristics of fathometer bottom returns in terms of water bottom type. Bottom typing methods study the returning energy from the water bottom using high frequency acoustic sources (20 – 200 kHz) [*Kloser et al.*, 2001] [*Bartholomä*, 2006]. The bottom returns include both specular reflections and scatter. Interpretations of the bottom returns yield sediment properties and geologic attributes [*Anderson et al.*, 2008].

The specular reflection is the spatially coherent energy reflected from the water-sediment interface, at an angle equal to the incident angle [*Chapman*, 2004]. The amplitude of a specular reflection is determined by the acoustic impedance contrast between the water and sediment; acoustic impedance is the product of the layer's density and acoustic velocity. The normal-incidence reflection coefficient (RC) in terms of pressure amplitude is:

$$RC = \frac{v_2\rho_2 - v_1\rho_1}{v_2\rho_2 + v_1\rho_1}, \quad (1)$$

where v_1 and ρ_1 are the water velocity and density respectively, and v_2 and ρ_2 are the sediment velocity and density, respectively. The remainder of the energy carried by the incident wave is transmitted through the interface. The normal-incidence transmission coefficient in terms of pressure amplitude is:

$$TC = \frac{2v_2\rho_2}{v_2\rho_2 + v_1\rho_1} \quad (2)$$

Scatter is a spatially incoherent return that radiates in all directions from surface roughness or inhomogeneities within the sediment [*Soukup and Odom*, 2009] [*Jones*, 1999]. The amplitude of scatter increases with increasing acoustic impedance contrast between the inhomogeneities within sediment and as the wavelength of the incident wave approaches the spatial dimensions of the inhomogeneities [*Gauss*, 2010] [*Lo and Inderwiesen*, 1994].

Acoustic fathometer sources produce narrow band signals in the range of 20 to 200 kHz and have wavelengths in water of 7.5 to 0.8 cm. Unconsolidated sediments contain inhomogeneities that are similar in size to the fathometer wavelengths, which is why there is a significant amount of scatter at these frequencies [*Toth et al.*, 1997].

Acoustic bottom typing methods are in standard use for many applications including defense (e.g., mine countermeasures), environmental (e.g., habitat mapping and protection), and economic (e.g., fisheries, mining) [*Hamilton*, 2001] [*Greene et al.*, 2007]. Roxann, an existing bottom typing method, nearly fulfills the objectives of this study. Roxann is a commercially available bottom typing method that uses existing on-ship fathometers to classify the texture of bottom sediments [*Schiagintweit*, 1993]. It works by analyzing energy in the first bottom return and first water-bottom multiple return (Figure 1). These returns contain both energy from specular reflections and scatter. Roxann estimates the RC by taking the ratio of the amplitude of the first return

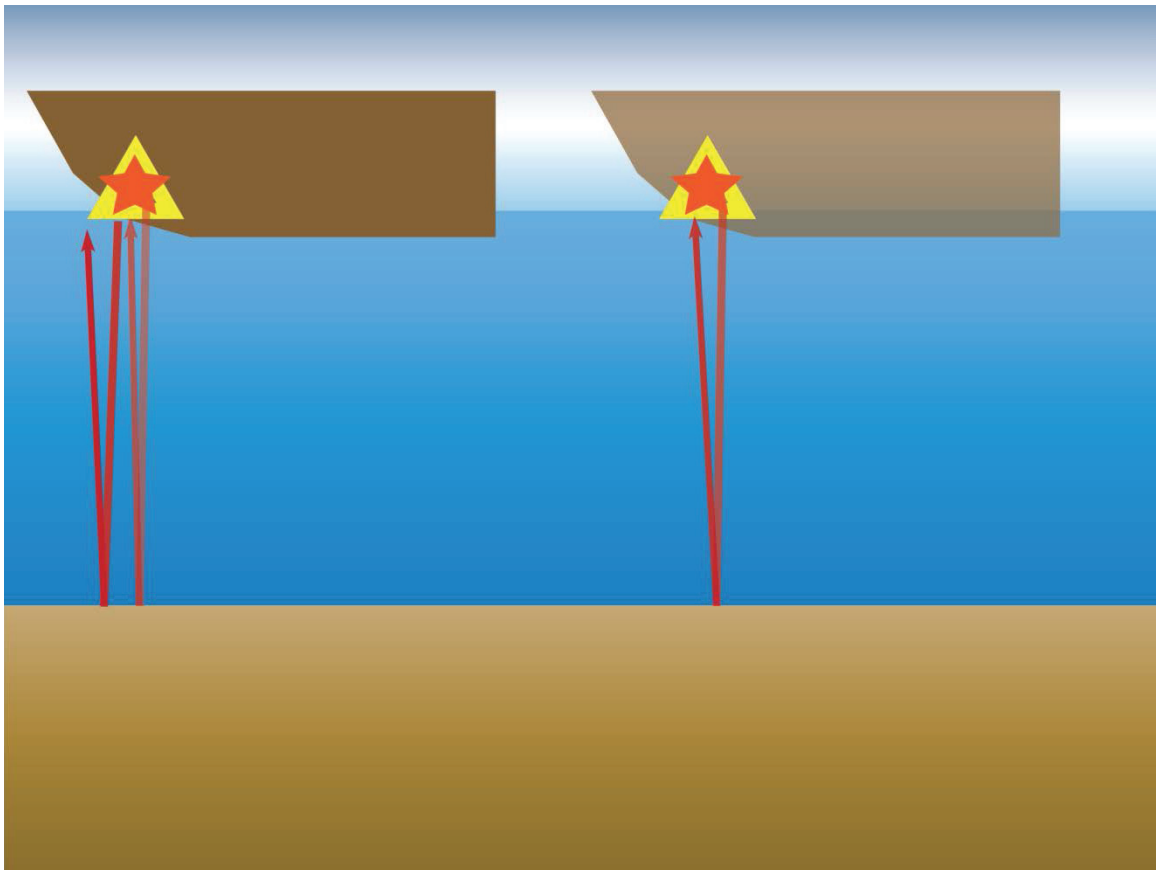

Figure 1. Roxann Reflection and First Multiple. The boat's fathometer is designated by the collocated yellow triangle (receiver) and orange star (source). The right side shows the ray path of the reflected wave, and the left side is the ray path of the first multiple.

and its first multiple. A large amount of scatter is generated due to the high frequency fathometer source in both the first reflection and its first multiple. The product of this method is an inaccurate representation of the RC; however, it provides a relative return amplitude that is correlated to water bottoms of clay, sand, coral, pebbles, sea grass, and other material types [Humborstad et al., 2004]. Roxann, as a bottom typing method, is not intended as a tool for quantifying material properties within a given sediment texture class. In general, Roxann and other existing bottom typing methods are not sufficiently accurate to determine material properties, require extensive local calibration with physical samples, and are too expensive for routine use in support of dredging operations [*Biffard*, 2011].

This study proposes an innovative acoustic method, RESDIPS (Remote Estimation of Sediment Density in Presence of Scatter), to extract the specular RC from returns containing scatter. Processing strategies, similar to those used for multi-channel reflection seismology, are tested to remove the scatter. The processing technique is evaluated using a finite element model to determine how well scatter is removed using the processing method. The sediment impedance is calculated from the recovered specular reflection and correlated to density through empirical relationship made by Neto (Figure 2). The estimated density of the sediment indicates whether fluid mud is present. Lastly, a field test is performed, as a proof of concept, to compare the calculated density to direct sampling.

2. Methods

The study uses a normal incidence acoustic survey to estimate the densities of soft sediments in shallow marine environments to assist in the planning of dredging

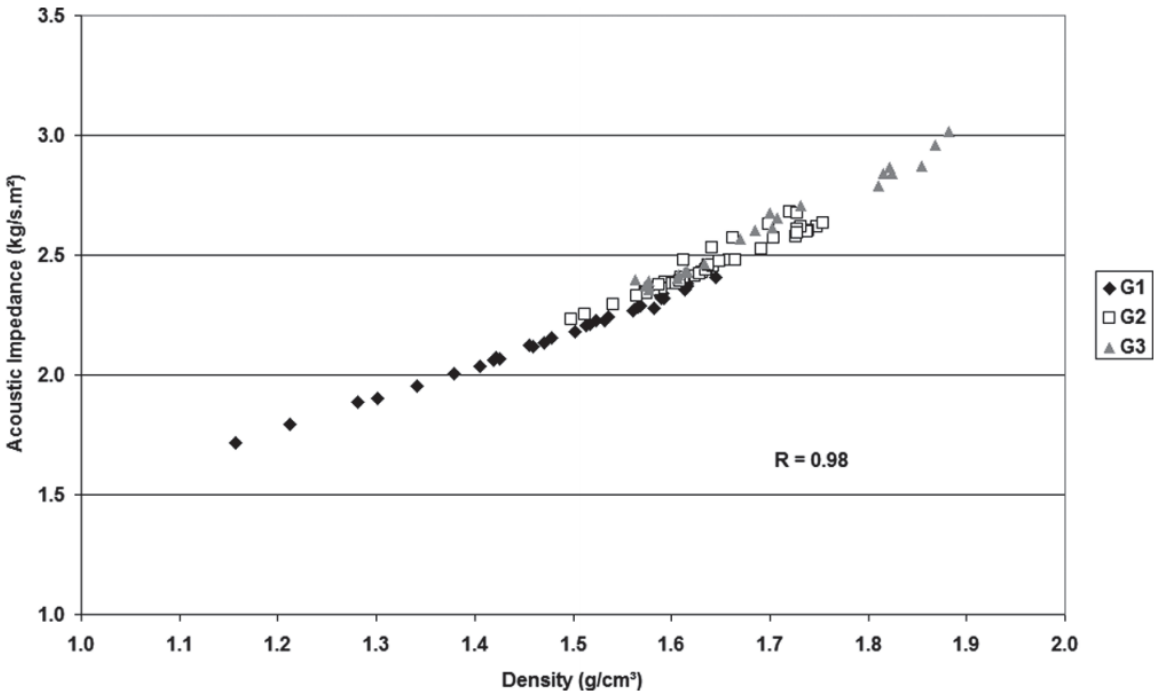

Figure 2. Acoustic Impedance versus Density. The three symbols labeled G1, G2, and G3 are based on the mud fraction of the material measured. G1, >80% mud, is the primary interest for this study. G2 contains >40% sand and gravel. Lastly, G3 contains coarser sediments, sand and gravel, making up more than 75% of the mud fraction.

operations. Using the RCs extracted from bottom returns and Equation 1, the impedance can be determined and correlated to density using Figure 2. The largest obstacle to this method is an accurate estimation of the RC in the presence of scatter (i.e. spatially incoherent noise). Stacking is the standard processing method used to remove incoherent noise. Stacking, as it is used in multi-channel reflection seismology, is performed by taking signals that originated from the same reflection point and adding them together. Stacking multiple seismic traces preserves coherent signals and removes incoherent noise. A finite element model is used to generate synthetic waves with scatter, which are then stacked and analyzed for residual noise.

2.1. Modeling

The finite element model is used because it provides a well constrained environment to generate synthetic waves with scatter. The model solves the two-dimensional acoustic wave equation (eq. 3) for pressure versus time.

$$\frac{\partial^2 p}{\partial x^2} - \frac{1}{c^2}\frac{\partial^2 p}{\partial t^2} = 0, \tag{3}$$

where x is position, p is pressure, t is time, and c is speed of propagation. The model elements are two centimeters in width and height. The model contains a water layer above a smooth sedimentary layer (Figure 3). The inputs for the densities and velocities of the water and sediment are: 1000 kg/m^3, 1500 m/s, 1500 kg/m^3, and 1600 m/s, respectively. The model has a pressure source and three receivers, which record the reflected wave, transmitted wave, and direct arrival. The model geometry is constructed so that the receivers record the waves after they travel 3 meters from the source. Equal travel distances removes the need for spherical corrections and pulse alignment. The 12 kHz source pulse is a tapered train of five sine wave cycles (Figure 4). The 12 kHz source frequency was chosen to reduce computation time, relative to the 16 kHz signal used in the field test. The finite model elements are two centimeters in width and height, and approximately 10 elements are required per wavelength to avoid numerical dispersion. A higher frequency source would have a shorter wavelength, requiring smaller elements. The 12 kHz source is 33 percent longer than a 16 kHz source, which allows elements to be 33 percent larger, requiring 78 percent fewer elements, and 78 percent less computation time. The total model size is 6 m wide by 10 m deep, with the top 4 m being water. Scatter could be generated through surface roughness or sediment

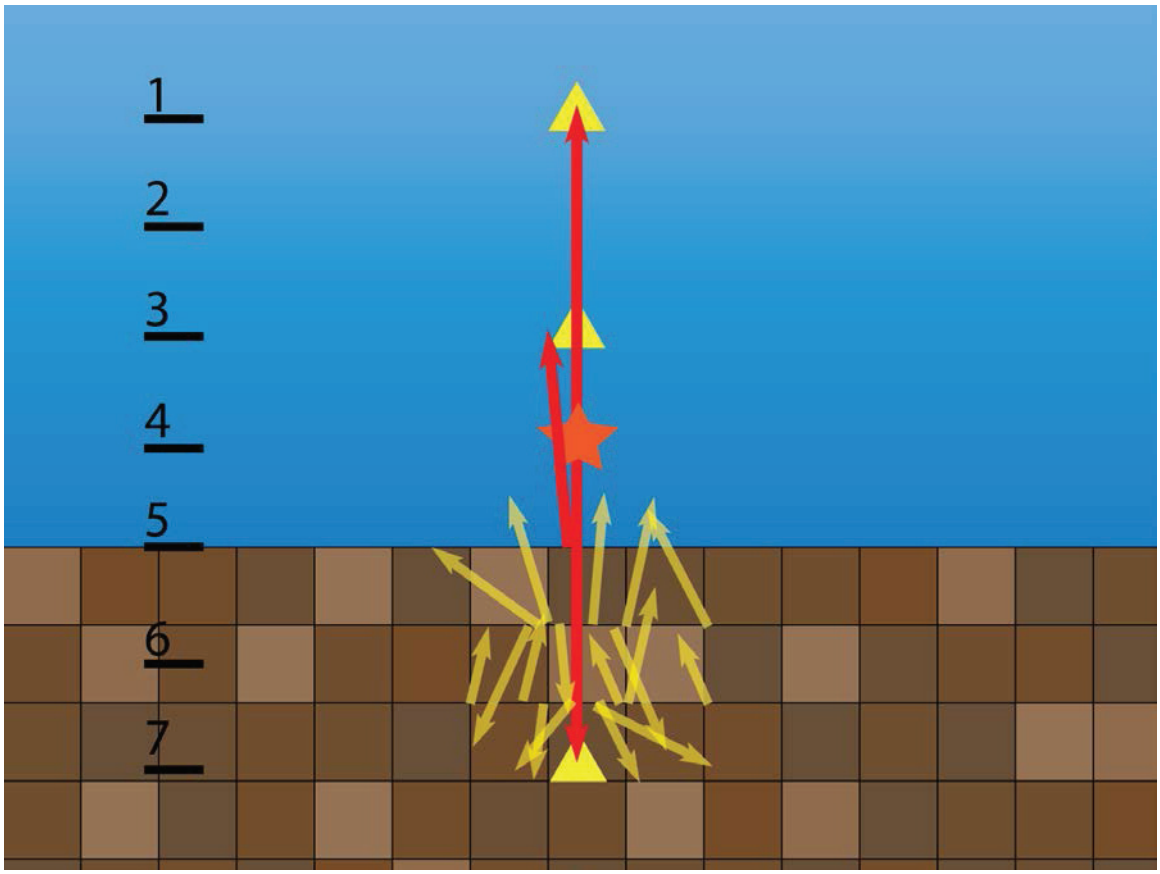

Figure 3. Model Configuration. The source is located at the orange star and receivers are located at the yellow triangles. Red arrows indicate the ray path from the source, after traveling 3 meters, to each of the hydrophones. Yellow arrows represent scatter. The shading of the sedimentary blocks indicates their impedance.

Figure 4. Source Wave Packet. This wave packet contains a train of 5 sine waves within half of a sine wave.

inhomogeneities. However, the water-fluid mud interface is expected to be smooth and relatively flat; therefore, surface scatter is ignored [*LeBlanc et al.*, 1995]. The inhomogeneities are generated by randomly perturbing the density and velocity (i.e.,

impedance) within rectangular blocks of elements. The block size and maximum percent perturbation are designated by user input. The average impedance of the model is unchanged because perturbations are random. As a result, the specular RC produced is consistent with the initial user inputs. The model is rebuilt 120 times using the same input parameters. Rebuilding the model generates a new sediment matrix and new random perturbations, which is how the model simulates a moving survey. The end product is a file with 120 pulses recorded at each of the three different receiver locations. Four block sizes are modeled, 2, 4, 10, and 20 cm, and each block's density and velocity is perturbed 10, 25, and 50 percent. In addition, an unperturbed model is run to test the precision of the model. The models investigated are indicated in Table 1.

Table 1. Model Input Combinations

Block Size	0%	10%	25%	50%
2cm	X	X	X	X
4cm		X	X	X
10cm		X	X	X
20cm		X	X	X

2.2. Acoustic Acquisition

The location for the initial field trial is Lake Lavon (Wylie, TX). The Texas Water Development Board surveyed Lake Lavon in 2011. They described the first 40 inches of the bottom sediment to be gelatinous mud without structure (i.e. fluid mud) [*Solis*, 2013]. The field trial system contains a 16 kHz omnidirectional piezoelectric source and a single, vertically offset hydrophone mounted 35 cm above the source. The source transducer and hydrophone are mounted on a frame that is towed 2 to 5 m above the water bottom. The 16 kHz source frequency is high enough to measure water depth

with sufficient accuracy and low enough to limit scatter. In addition, the 16 kHz source has a frequency that is low enough to penetrate through the fluid mud to the more solid bottom. Reflections from both the fluid mud bottom and solid bottom are important to determine the fluid mud thickness. The source pulse generated is roughly a 9 cm wave packet with a tapered train of five sine wave cycles, for a total pulse length of 0.3125 milliseconds. The source wavelet is similar in shape to the model source, but higher in frequency (Figure 4). The analog signal from the hydrophone is recorded with a 21 bit analog to digital converter with a 10 microsecond sample rate and a total record length of 0.03 seconds is produced. The 21 bit converter is required due to the relative amplitude difference between the direct arrival and the reflected waves.

RESDIPS remotely estimates sediment density through a novel use of standard methods in conjunction with the empirical correlation in Figure 2. The hydrophone collects the direct arrival (i.e. source pulse wave) and the water bottom return. The water bottom return contains the specular reflection and scatter. The amplitude of the specular reflection divided by the amplitude of the direct arrival produces the sediment RC (eq. 1). The acoustic velocity and the density of the water are easily measured and are nearly constant and the acoustic velocity of the fluid mud is close to that of water. This means that the amplitude of the bottom reflections correlate to the sediment density. This connection allows RESDIPS to estimate the density of sediments using Neto's empirical correlation. The success of RESDIPS is based upon an accurate RC and applicable empirical correlation.

Core samples are retrieved along the acoustic survey lines. The top 12 cm of the core is used for analysis. Three sub samples are taken within the 12 cm interval and

averaged. The bulk density is measured using a cylindrical cup with a 2.75 cm radius and 4 cm length. The cup is weighed empty and full, and the two weights are subtracted and divided by the volume. Water content by weight is determined by weighing the sample wet, oven-drying the sample for 24 hours, and weighing the dry sample.

2.3. Data Processing

The Lake Lavon and model data are processed using a number of small computer programs developed to perform various tasks. The short segments of the acoustic recordings containing the bottom returns from the Lavon data are manually extracted, and the model data returns are extracted based on the 3 m travel time. The extracted interval is chosen to start before the arrival and extend beyond the end of the expected pulse length by 30%. This step is performed because the length of the data is important when performing the next step, cross correlation. Cross correlation slides an ideal model pulse along the recorded pulses and multiplies the two; the time shift resulting in the greatest cross correlation value is chosen as the best fit arrival time. Starting at the best fit arrival time, a received pulse is extracted of the same length as the expected outgoing pulse. The extracted pulse is thus aligned and ready to be stacked. Stacking is a common industry method, but it is typically performed with common mid-point (CMP) data from multi-channel surveys (Figure 5) [*Moini and Gazdag*, 1989]. Since this study only records normal incidence reflections, stacking is performed by adding water bottom returns from different locations but along the same interface (Figure 6). Each trial data line is collected over short intervals of the water bottom. This means the bottom returns are from similar impedance contrasts and similar specular reflections should be found. The stacking process takes the first time sample from every trace, adds them together, and

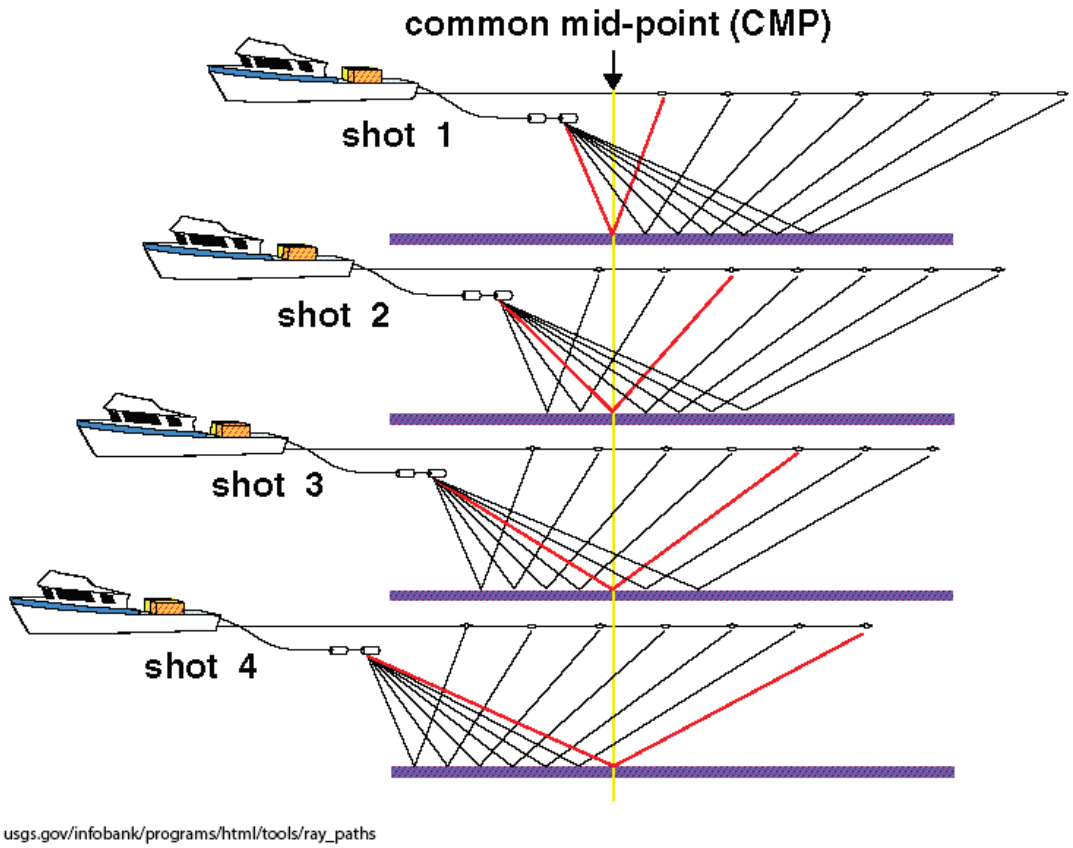

Figure 5. CDP Stacking. The following shows four shot points over a CDP. The ray path reflecting off the CDP for each shot is designated by a red line. The yellow vertical line traces through the CDP.

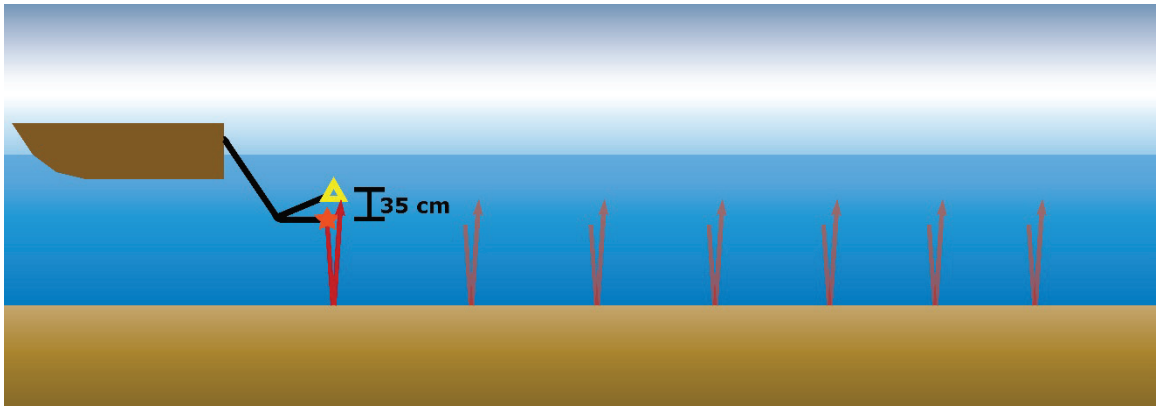

Figure 6. Field Survey Ray Paths. The following shows the ray paths of the field survey at multiple shot points. The yellow triangle is the hydrophone and the orange star is the source.

divides by the number of points that are added; this value is the amplitude of the first point of the stacked trace. This process is repeated for each time sample in the pulse. The stacking process in equation form is:

$$S_n = \frac{\sum_{i=1}^{N} A_n(i)}{N}, \tag{4}$$

where S_n is the stacked amplitude, n is the time sample number, N is the number of traces in the stack, and $A_n(i)$ is the trace amplitude of the nth time sample of the ith trace.

For the case of a perfectly coherent signal and random noise, the stacking process improves the signal to noise ratio (SNR) by the product of the square root of the number of traces stacked. The root mean square (RMS) is used to calculate the energy of the stacked pulse. The equation for RMS is:

$$x_{RMS} = \sqrt{\frac{1}{N}\sum_{i=1}^{N} x_i^2} \tag{5}$$

where N is the number of data points and x_i is the data point amplitude. The direct and reflected waves, in the Lake Lavon data, travel different distances. Wave amplitude decreases as a function of distance. The reflected wave and direct arrival are spherically corrected to scale them at a unit travel distance. This is done by multiplying the RMS values with their travel time and velocity of the medium. Then, the ratio of the reflected wave and the direct arrival produces the apparent RC.

The data are also run through a separate workflow without stacking to provide individual, trace by trace, RCs to compare with the stacked data. This workflow took the RMS for each individual direct arrival and reflected wave. The Lavon data also required a spherical spreading correction. This work flow does not remove scatter, and thus, the

results are similar to those produced by the Roxann approach applied to lower frequency data, but without making use of the water bottom multiple. The acoustic impedance of the sediment is then calculated using the RC, and the assumed velocity and density of water, 1480 m/s and 1000 kg/m^3, respectively. Lastly, using the calculated impedance in conjunction with the correlation in Figure 2, the density of the sediment is estimated.

3. Results

The results are arranged to first show the model results and the effects of stacking signals with scatter. Second, the Lake Lavon field test data is stacked to remove scatter and the results are used to estimate sediment densities. Lastly, the core analysis is presented as a direct measurement of the sediment in the reservoir.

3.1. Model Results

Example returns from each of the virtual receivers in the model are shown in Figure 7. These returns are full records and include portions of the wave that will be clipped during wave extraction. The top receiver collects the direct arrival and a small amount of numerical ringing, which trails the wave packet. The middle receiver shows an early amplitude spike from the direct wave passing by, followed by the bottom return and trailing scatter. All waves travel the same distance, however the energy loss from the interface and inhomogeneities is visible in the amplitude of the transmitted wave collected at the bottom receiver.

Ten extracted synthetic reflections and their stacked result are shown in Figure 8. Different scatter frequencies and amplitudes are visible within each of the pulses. The smooth wave packet that emerges demonstrates the effectiveness of stacking.

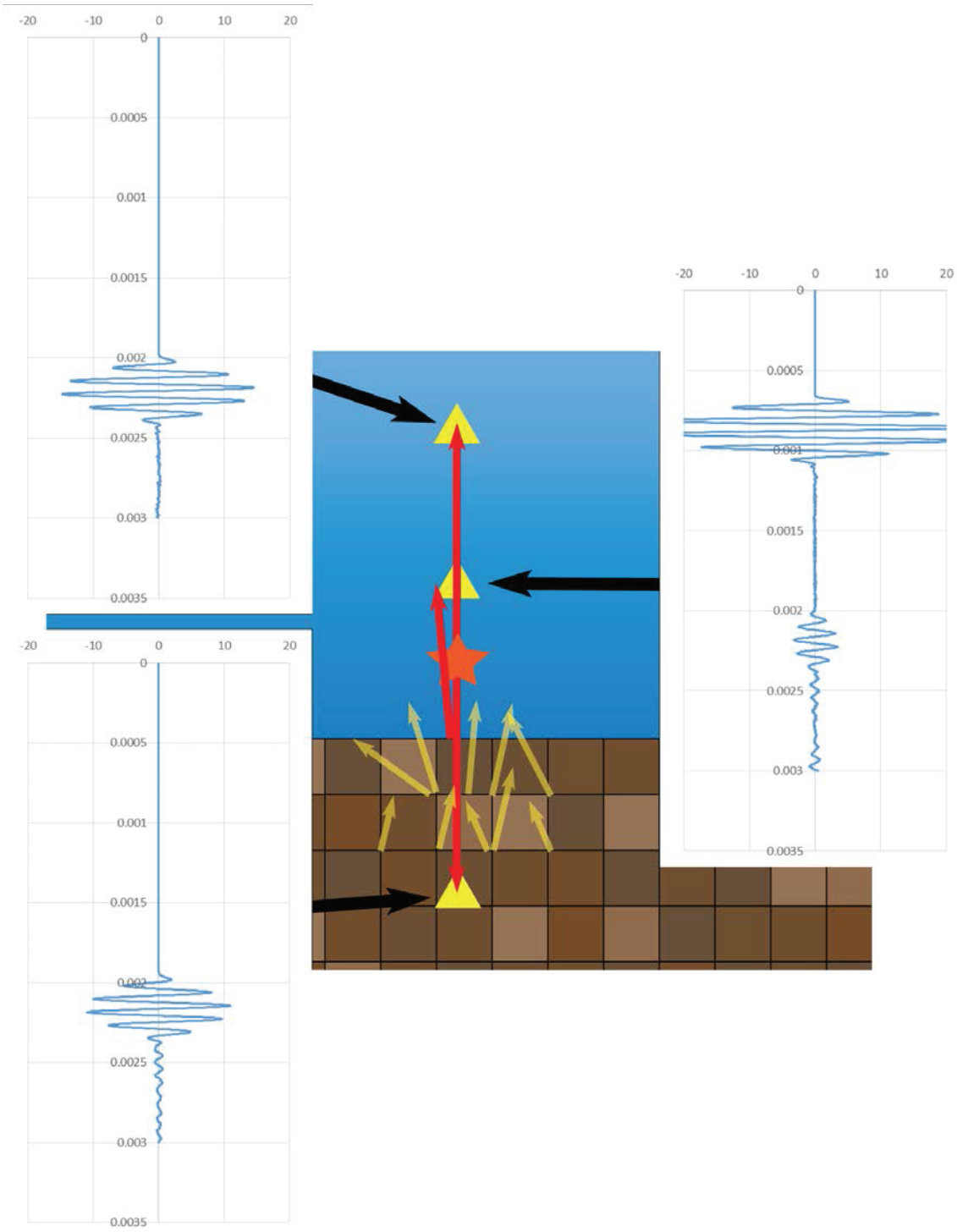

Figure 7. Modeled Full Synthetic Waves. Here the full data collection from each virtual receiver (yellow triangle) are shown. The source is designated by the orange star.

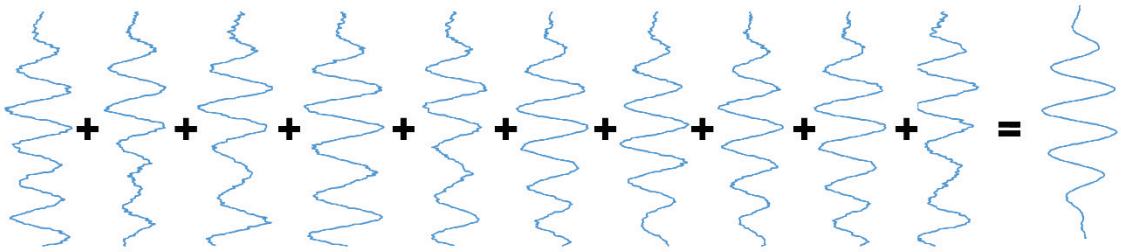

Figure 8. Stacked Model Traces. These 10 raw traces were the first 10 traces generated by the 2 cm 10 percent model. The resulting stack trace from these 10 traces is shown on the right.

A total of 13 model runs were completed in this study. Examples from the unperturbed model, and the perturbed 2 cm and 10 cm models are described in detail below. As previously stated, the normal parameters for all the models' water and sediment, densities and velocities are: 1000 kg/m^3 and 1500 m/s, and 1500 kg/m^3 and 1600 m/s, respectively; these produce a RC of 0.231 and a TC of 1.231. These reflection and transmission coefficients are the expected values in the unperturbed model results in Figures 9 and 10, based on the analytical solution for the reflection and transmission coefficients (Eq. 1 and 2). These figures show the reflection and transmission coefficients, with and without stacking, computed from 120 different model runs with identical input parameters and without perturbation. Even though volume perturbations are not being used to generate scatter, the numerical error within the finite element method perturbs the result. Most individual (i.e., unstacked) values deviate less than five percent from the expected value. While the results after 20 stacks contain an error of one percent. Therefore, a numerical error of about one percent can be expected in the models after stacking.

The results from the perturbed 2 cm and 10 cm models are shown in Figures 11 through 14. These two block sizes are examined further due to their dimensions in

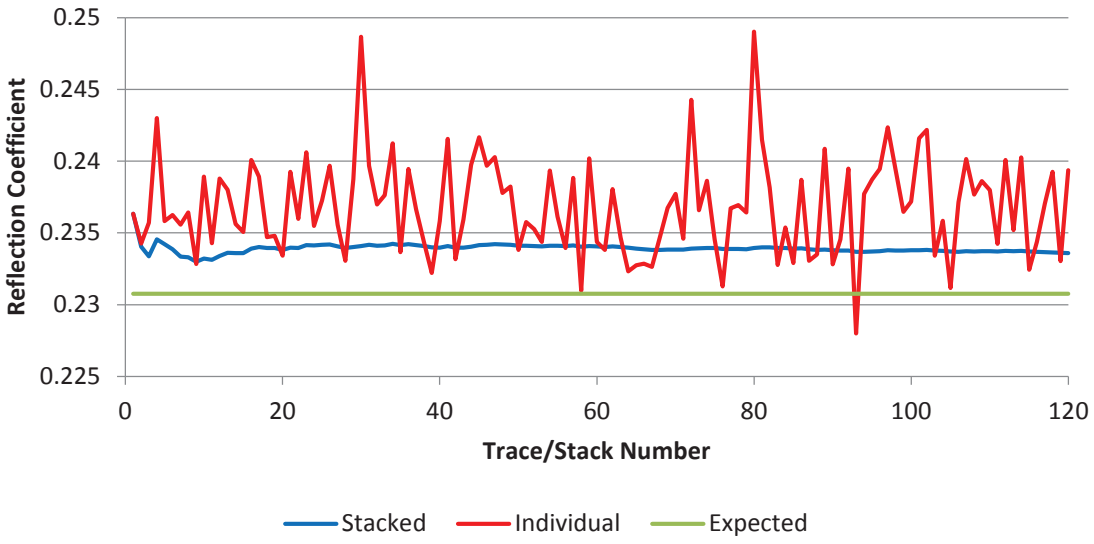

Figure 9. Unperturbed model RC. The green line is a calculated value based on the material properties, the red line is individual modeled reflection amplitudes, and the blue line is the amplitude of the reflection after stacking different numbers of reflections from independently perturbed models.

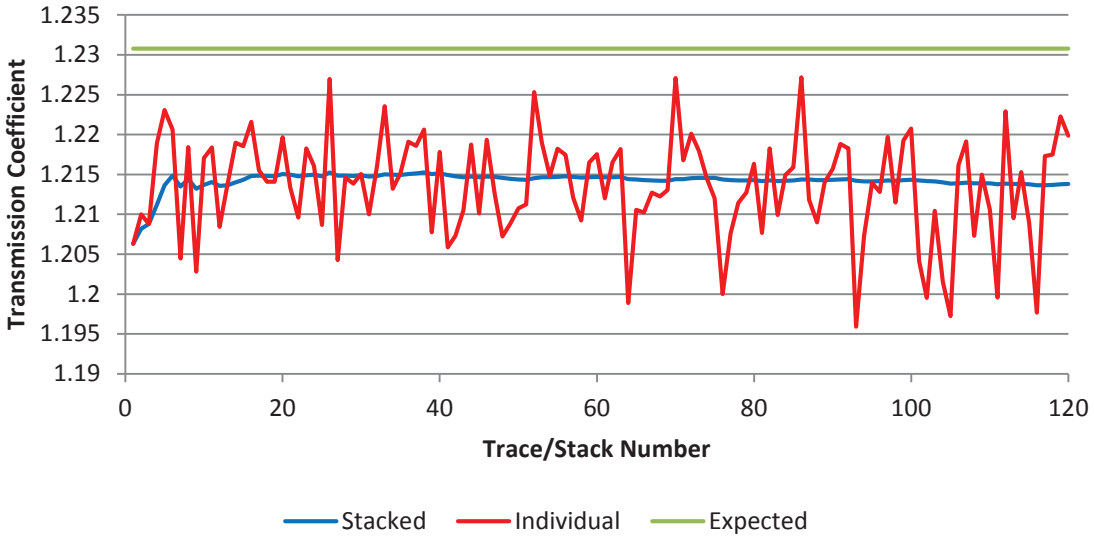

Figure 10. Unperturbed model TC. The green line is a calculated value based on the material properties, the red line is individual modeled reflection amplitudes and the blue line is the amplitude of the reflection after stacking different numbers of reflections from independently perturbed models.

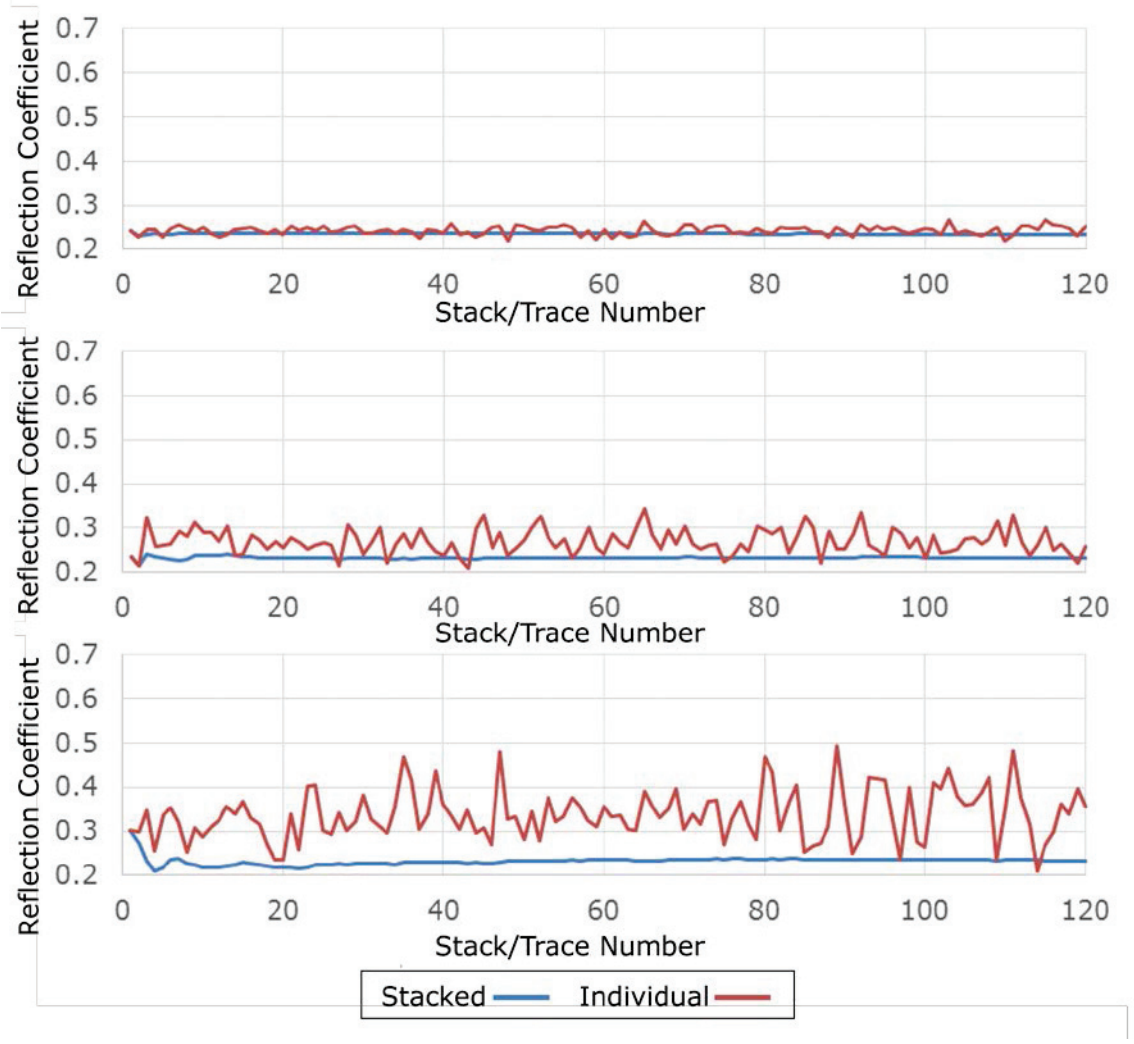

Figure 11. Model Data 2cm RC. The order from top to bottom is 10, 25, and 50% perturbation. Each of the graphs are scaled identically to show the amount of scatter generated.

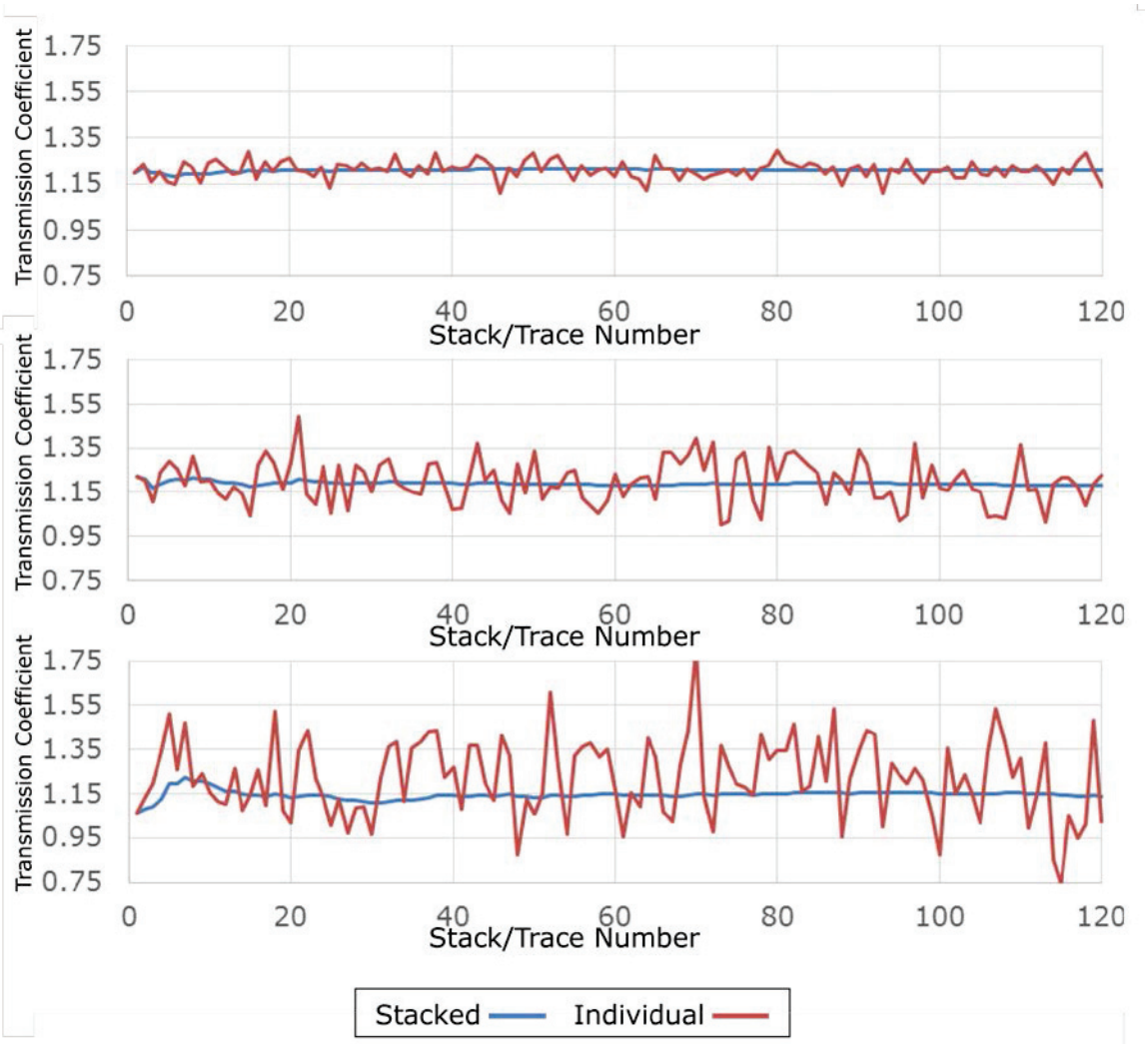

Figure 12. Model 2 cm TC. The order from top to bottom is 10, 25, and 50% perturbation.

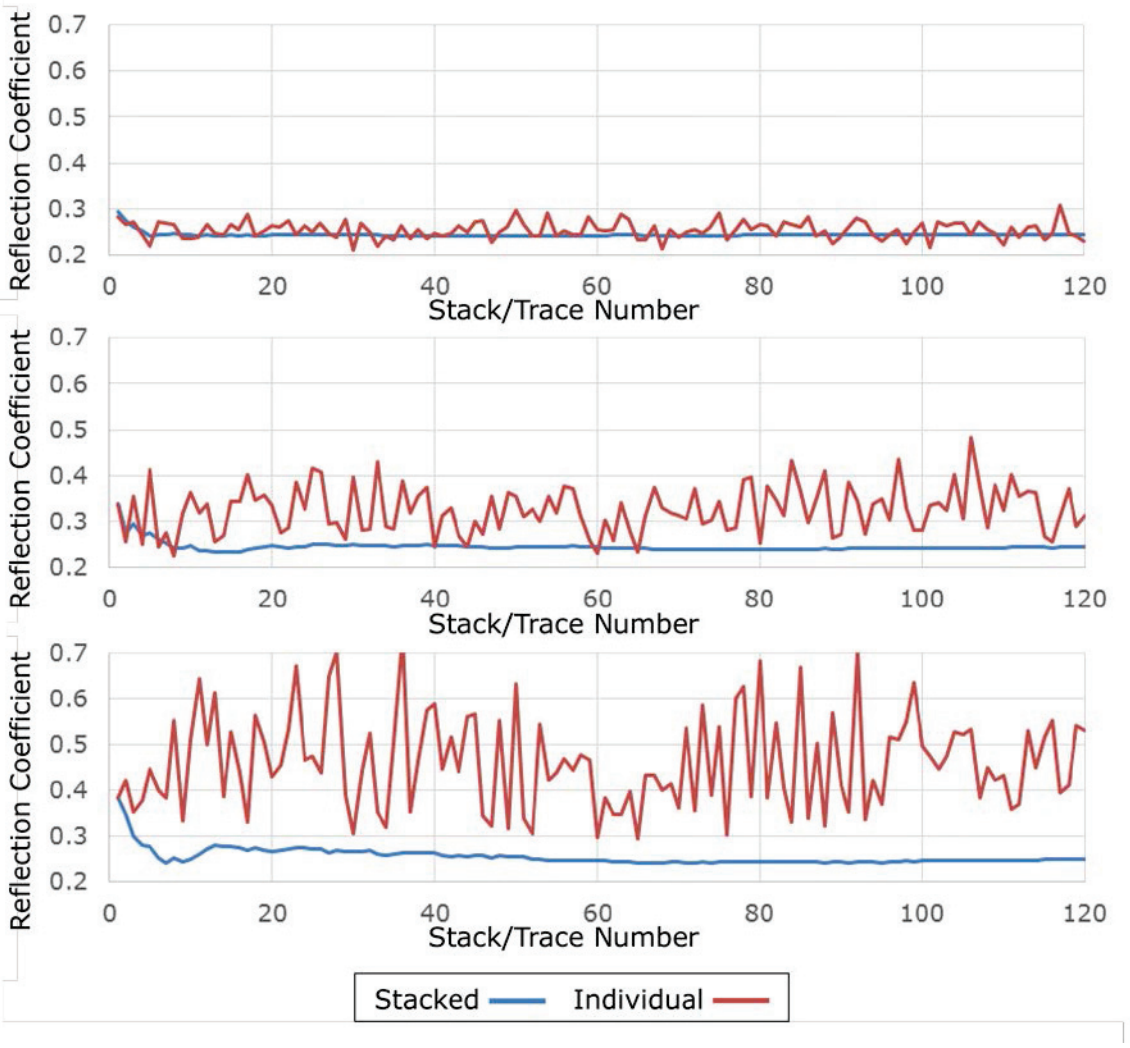

Figure 13. Model 10 cm RC. The order from top to bottom is 10, 25, and 50% perturbation.

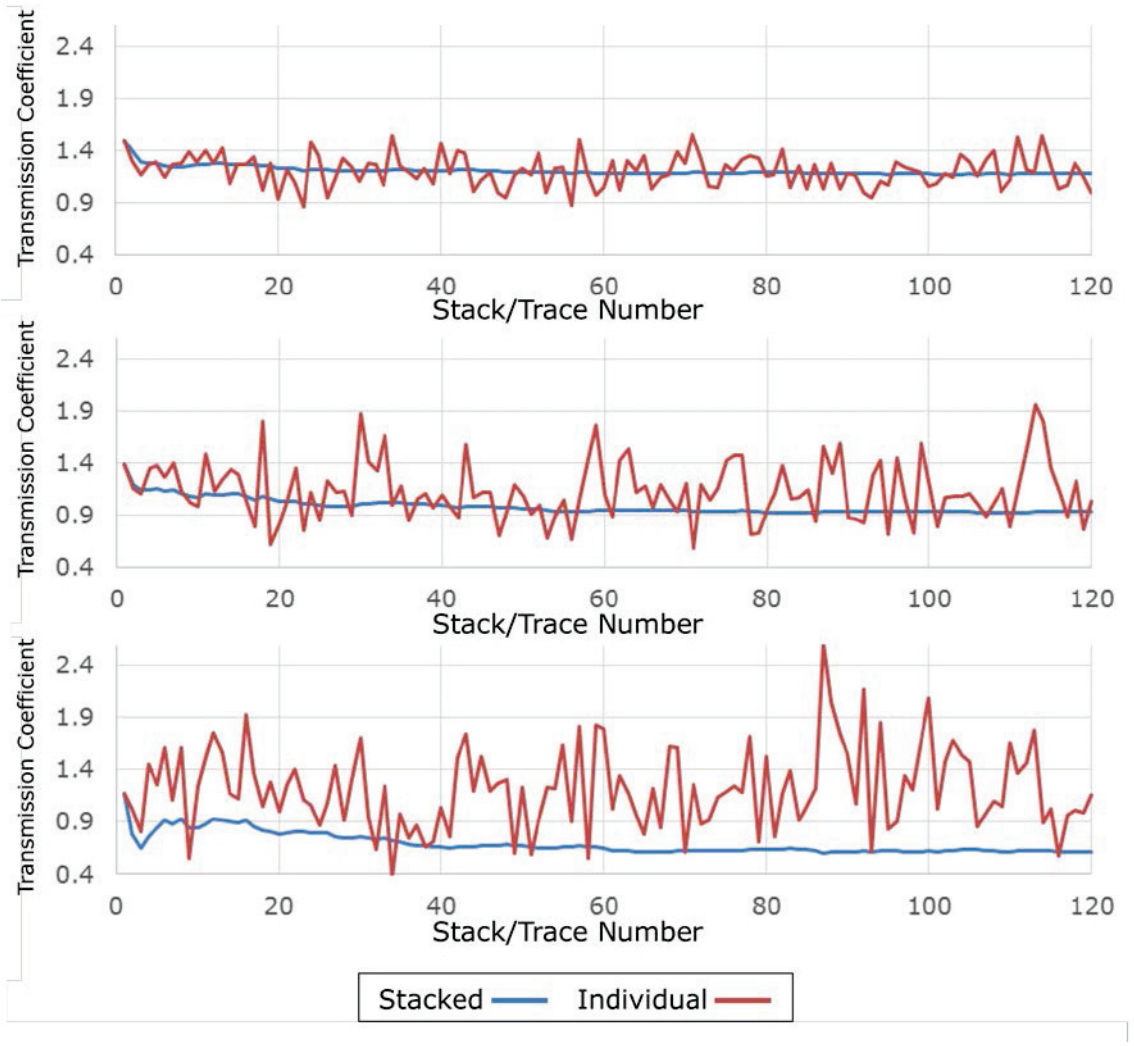

Figure 14. Model 10 cm TC. The order from top to bottom is 10, 25, and 50% perturbation.

relation to the 13 cm source wavelength. The 2 cm model, should contain a small amount of scatter because the size of the inhomogeneities is a fraction of the 13 cm signal wavelength. Conversely, the 10 cm model approaches the dimensions of the signal wavelength, which should increase the amount of scatter. The following figures show the calculated apparent RCs of both individual traces and stacked traces. The results from the 2 cm model, with perturbations of 10, 25, and 50 percent, are shown in Figure 11. Individual traces show the total energy from a combination of specular reflections and scatter. The stacked traces display the RC with removal of scatter. Notice, an increase in the number of stacked traces brings the RC closer to 0.231, the expected RC. After ten stacks the 10 and 25 percent perturbation model RCs have an error of less than two percent. The 50 percent perturbation model has more scatter and the RC error is seven percent after 20 stacks.

The transmitted wave is recorded because scattered energy is partitioned from this wave and the diminished energy recorded confirms the generation of scatter. Figure 12 shows the stacked and unstacked TCs for each of the perturbations. The stacked values show that an increase in perturbation decreases the amount of energy transmitted due to the extra scatter generated at the inhomogeneities. The individual traces TC results show fluctuations similar to the RC results which can also be attributed to scatter. Furthermore, individual TCs that exceed unity (i.e., more than the source energy) can only be explained through extra energy from scatter.

The 10 cm block size RC's results are similar to the 2 cm model, but with an increase in scatter for all models (Figure 13). The stacking method is shown to be effective in these conditions, even though inhomogeneities approach the dimensions of

the source wavelength, which generates maximum scatter. After 20 stacks, the 10 and 25 percent RC errors are only one and five percent, respectively. The transmission results in Figure 14 also show similar trends to the 2 cm model, again with the exception of additional scatter in the 10 cm results. The extra scatter in the 10 cm model results in larger individual trace RC and TC values.

Tables 2 and 3 display the results from all of the model runs at selected stacking intervals. As expected, the 20 cm model contains less scatter than the 10 cm model, due to the relative block size compared to the 13 cm source wavelength. Along the same lines, the results of the 5 cm model indicate less scatter than the 10 cm model, but more than the 2 cm model. Tables 2 and 3 also reveal that large perturbations and large block sizes contain residual scatter creating considerable errors, even after a large number of traces have been stacked. However, the individual RC SNRs for the 50 percent perturbation 10 cm blocks shown in Figure 13 indicate that there is twice as much noise as signal. The resulting stacked line is remarkably smooth, and falls within six percent of the expected RC by the 60^{th} stack. The 60^{th} stack of this poor noisy data should produce a SNR of roughly 4, while individual RCs are overestimated by 30 to 300 percent.

3.2. Lake Lavon Results

Four acoustic lines and one core are collected during the field test. The four lines are acquired with the transducer towed at various heights above the water bottom in the same region of the lake. The data from one line is displayed in Figure 15. The space between the red and yellow lines is an example of the area where bottom returns are extracted. Figure 16 displays ten of these extracted returns from a single line and their

Table 2. Model Data 2 cm and 4 cm.

Stack	2cm 10% RC	RC % error	2cm 25% RC	RC % error	2cm 50% RC	RC % error	4cm 10% RC	RC % error	4cm 25% RC	RC % error	4cm 50% RC	RC % error
1	0.239	3.754	0.232	0.332	0.300	29.965	0.252	9.343	0.296	28.326	0.422	83.056
2	0.229	0.981	0.212	8.090	0.269	16.751	0.243	5.172	0.284	23.099	0.329	42.472
3	0.231	0.013	0.239	3.494	0.230	0.242	0.242	5.068	0.284	22.859	0.311	34.603
4	0.232	0.607	0.233	0.813	0.206	10.612	0.249	7.766	0.258	11.715	0.288	24.814
5	0.229	0.612	0.229	0.836	0.216	6.249	0.240	4.065	0.263	13.964	0.282	22.164
6	0.231	0.247	0.227	1.442	0.232	0.471	0.234	1.500	0.262	13.425	0.301	30.343
7	0.234	1.371	0.225	2.613	0.236	2.384	0.237	2.580	0.255	10.290	0.282	22.289
8	0.234	1.498	0.227	1.487	0.225	2.448	0.236	2.232	0.251	8.738	0.296	28.052
9	0.234	1.327	0.235	1.647	0.222	3.930	0.237	2.911	0.250	8.447	0.294	27.207
10	0.234	1.372	0.235	1.676	0.215	6.629	0.235	1.951	0.252	9.052	0.265	14.678
20	0.232	0.520	0.229	0.882	0.215	6.859	0.227	1.435	0.243	5.358	0.226	2.014
35	0.233	0.911	0.228	1.221	0.227	1.738	0.228	1.328	0.248	7.576	0.225	2.630
60	0.232	0.582	0.230	0.436	0.233	1.057	0.228	1.104	0.239	3.662	0.225	2.494
90	0.231	0.241	0.230	0.249	0.234	1.212	0.229	0.697	0.236	2.217	0.217	6.081
120	0.231	0.216	0.229	0.758	0.230	0.152	0.231	0.076	0.236	2.280	0.219	5.179

Table 3. Model Data 10 cm and 20 cm.

Stack	10cm 10% RC	RC % error	10cm 25% RC	RC % error	10cm 50% RC	RC % error	20cm 10% RC	RC % error	20cm 25% RC	RC % error	20cm 50% RC	RC % error
1	0.280	21.325	0.337	45.897	0.380	64.571	0.241	4.420	0.345	49.624	0.238	3.028
2	0.260	12.795	0.273	18.221	0.345	49.436	0.227	1.616	0.269	16.599	0.287	24.420
3	0.246	6.658	0.292	26.686	0.299	29.555	0.225	2.414	0.228	1.034	0.243	5.420
4	0.238	3.156	0.267	15.569	0.278	20.390	0.233	0.839	0.219	4.919	0.290	25.739
5	0.229	0.952	0.273	18.104	0.276	19.434	0.221	4.090	0.212	8.148	0.271	17.550
6	0.232	0.421	0.257	11.495	0.249	8.038	0.226	1.904	0.210	8.991	0.275	19.290
7	0.230	0.183	0.250	8.381	0.239	3.730	0.229	0.878	0.208	9.983	0.289	25.068
8	0.233	1.044	0.240	3.910	0.250	8.158	0.228	1.318	0.210	8.905	0.275	18.998
9	0.231	0.277	0.239	3.750	0.244	5.559	0.228	1.033	0.210	9.109	0.265	15.009
10	0.230	0.477	0.243	5.237	0.246	6.809	0.231	0.270	0.213	7.655	0.253	9.686
20	0.230	0.443	0.243	5.300	0.265	14.830	0.232	0.434	0.212	7.917	0.224	2.981
35	0.229	0.942	0.242	5.029	0.260	12.543	0.234	1.495	0.219	4.896	0.225	2.315
60	0.229	0.601	0.241	4.346	0.244	5.843	0.232	0.697	0.226	1.993	0.234	1.451
90	0.230	0.352	0.237	2.594	0.241	4.586	0.230	0.523	0.227	1.565	0.234	1.581
120	0.230	0.463	0.240	4.182	0.247	6.885	0.232	0.362	0.228	1.405	0.242	4.745

stacked result. Each return has been trimmed and aligned. The stacked result emerges as a relatively clean pulse with minimal scatter.

The stacked and individual RC results from the four Lake Lavon survey lines are shown in Figure 17. The data presented are spherically corrected. The stacked and

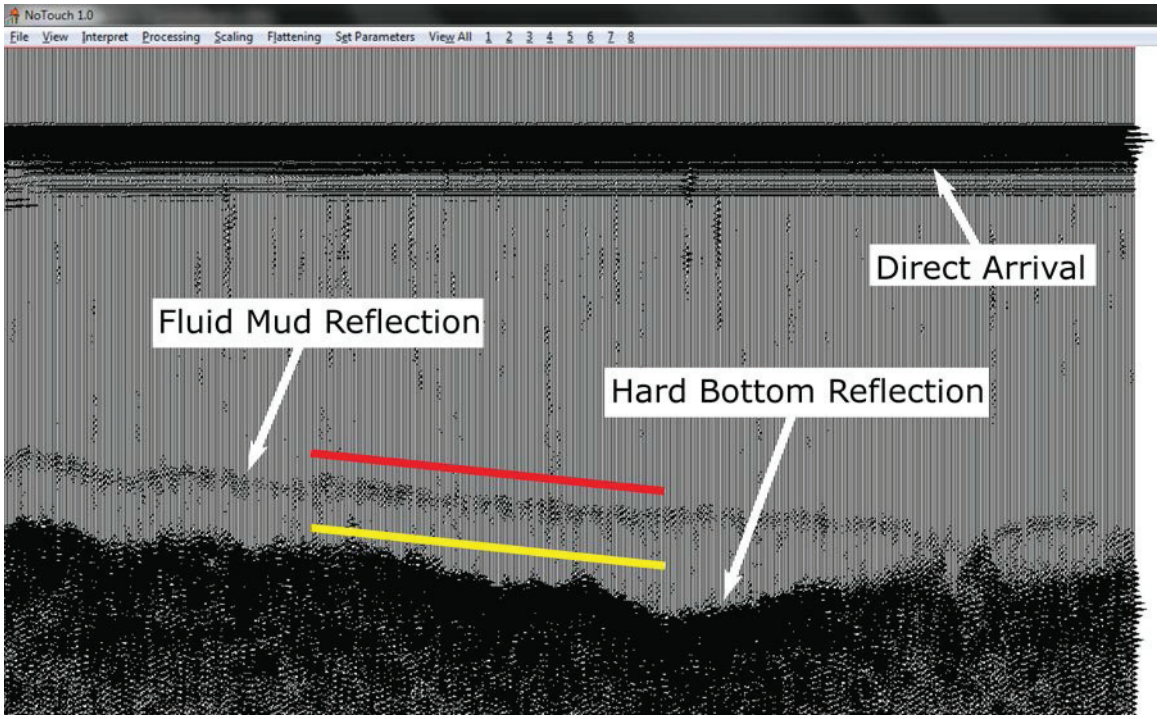

Figure 15. Lavon Survey Line Data. This is similar to a side profile of the lake with hundreds of individual traces side by side. Each trace runs vertically where the top is the beginning of the trace. The red and yellow lines are an example of the manually designated picking interval where the traces will be extracted.

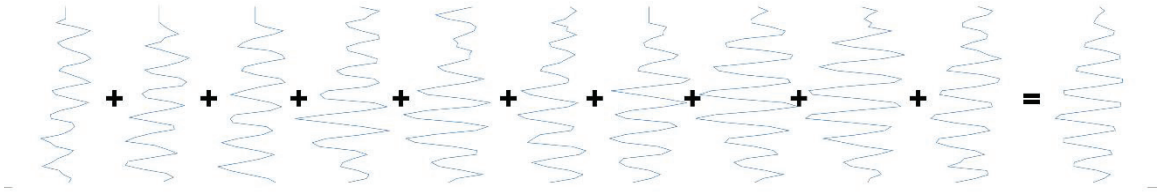

Figure 16. Lake Lavon Waves Stacked. Similar the model stacking example, again after only 10 stacks, a clean wave emerges.

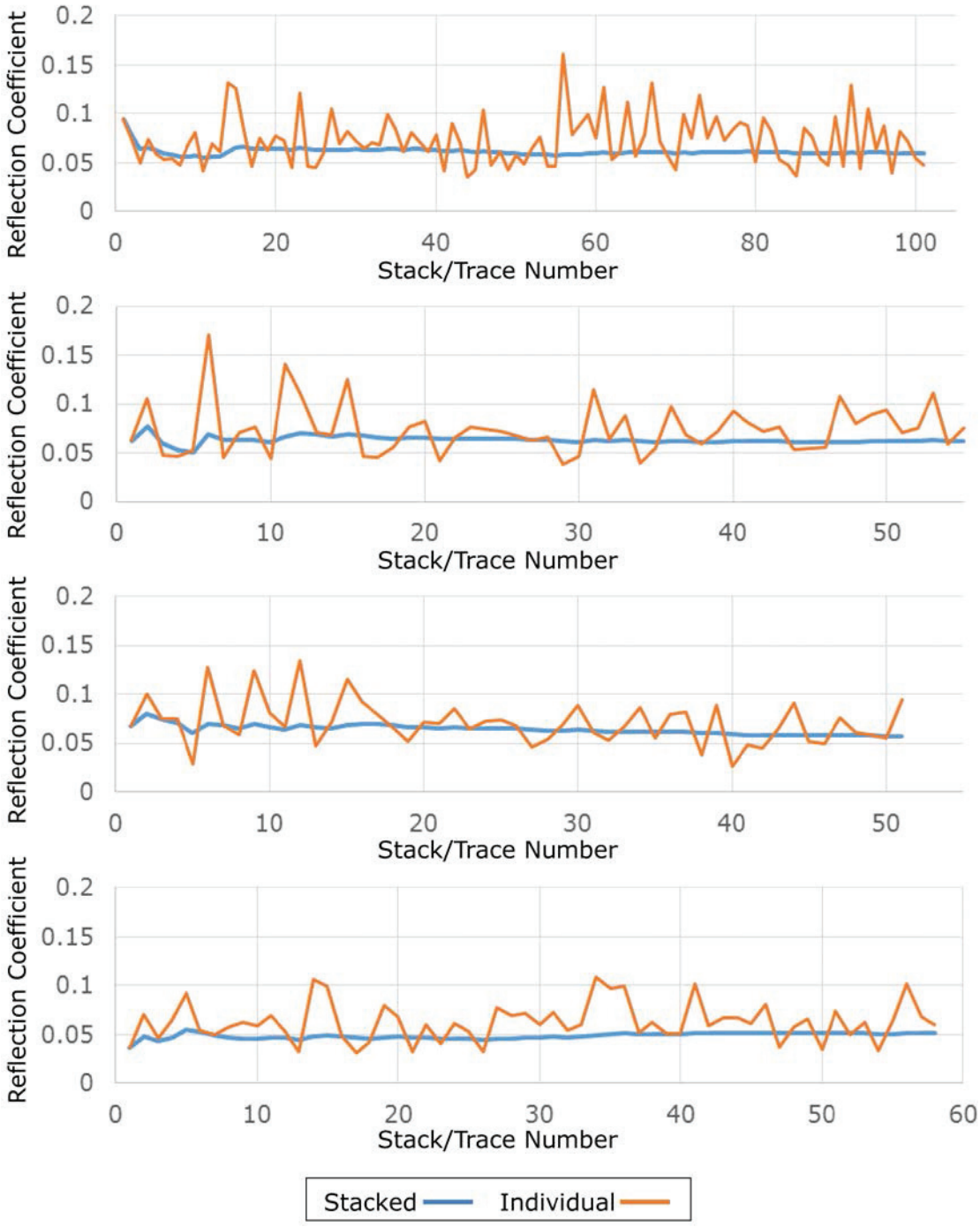

Figure 17. Lavon Survey Lines. From top to bottom, these are surveys one through four.

individual field traces look similar to the model results. This means there is scatter within the data and stacking is removing the scatter. Furthermore, the stacked RC is fairly smooth after only 10-20 traces are stacked. There also appears to be a fair amount of scatter in the data with individual RC swings up to three times that of the stacked RC. Overall, each line has similar stacked RC results in the presence of varying amount of scatter.

The results from stacked and individual traces for each of the four acoustic lines are shown in Table 4. Columns labeled with (i) are individual traces. The densities are estimated using Figure 2 and the steps outlined in the methods section. The densities are color coded based on the presence of fluid mud; green means fluid mud is present with a density of 1.1 or less, then transitioning to yellow indicating probable fluid mud with a density of 1.2, and finally red means a hard bottom with densities above 1.3. After 10 stacks the computed densities for each of the four surveys indicate fluid mud, but individual traces irregularly designate hard bottoms because the RC is over estimated from the addition of scatter.

3.3. Core Measurements

A single core is acquired in the vicinity of the survey lines. The top 12 cm of the core is used for density analysis; from the 12 cm section, three sub-samples are evaluated and the measured values are averaged. The measurements determined an average bulk density of 1.23 g/cm^3, and a water content between 68.5-71.7 percent, with an average of 70.1 percent. These values are at the top of the range of what would be expected for fluid mud which has been undisturbed and partially dewatered.

Table 4. Lake Lavon Data.

Trace	RC1	Density	RC1(i)	Density(i)	RC2	Density	RC2(i)	Density(i)	RC3	Density	RC3(i)	Density(i)	RC4	Density	RC4(i)	Density(i)
1	0.094	1.222	0.094	1.222	0.062	1.153	0.062	1.153	0.068	1.164	0.068	1.164	0.037	1.102	0.037	1.102
2	0.078	1.187	0.075	1.179	0.078	1.185	0.106	1.247	0.080	1.191	0.101	1.235	0.048	1.124	0.070	1.170
3	0.065	1.158	0.050	1.128	0.060	1.148	0.048	1.124	0.074	1.177	0.075	1.179	0.043	1.114	0.047	1.122
4	0.066	1.160	0.074	1.177	0.053	1.133	0.046	1.121	0.071	1.171	0.075	1.180	0.048	1.123	0.065	1.159
5	0.063	1.155	0.059	1.147	0.051	1.130	0.053	1.133	0.060	1.149	0.029	1.086	0.055	1.137	0.092	1.216
6	0.060	1.148	0.054	1.136	0.069	1.168	0.170	1.405	0.070	1.169	0.127	1.297	0.052	1.133	0.055	1.137
7	0.058	1.144	0.055	1.138	0.064	1.156	0.045	1.119	0.069	1.166	0.068	1.165	0.049	1.126	0.049	1.127
8	0.056	1.141	0.047	1.122	0.063	1.155	0.071	1.172	0.065	1.159	0.059	1.147	0.047	1.122	0.058	1.144
9	0.056	1.141	0.068	1.164	0.064	1.156	0.076	1.182	0.070	1.168	0.124	1.289	0.046	1.120	0.062	1.153
10	0.058	1.144	0.081	1.192	0.061	1.150	0.044	1.116	0.067	1.162	0.081	1.192	0.046	1.120	0.059	1.146
15	0.066	1.160	0.125	1.292	0.070	1.168	0.124	1.290	0.068	1.165	0.115	1.268	0.050	1.127	0.099	1.232
20	0.065	1.158	0.078	1.186	0.066	1.161	0.082	1.195	0.066	1.161	0.072	1.173	0.048	1.124	0.068	1.165
25	0.063	1.154	0.045	1.118	0.064	1.157	0.072	1.174	0.065	1.159	0.074	1.178	0.046	1.120	0.053	1.135
30	0.064	1.156	0.072	1.173	0.062	1.152	0.047	1.122	0.064	1.156	0.089	1.209	0.047	1.122	0.060	1.149
35	0.064	1.157	0.085	1.200	0.062	1.151	0.055	1.137	0.061	1.151	0.055	1.139	0.050	1.128	0.097	1.227
40	0.063	1.155	0.079	1.188	0.062	1.152	0.092	1.217	0.059	1.147	0.026	1.082	0.051	1.129	0.050	1.129
45	0.061	1.150	0.043	1.115	0.061	1.150	0.054	1.137	0.058	1.145	0.052	1.132	0.052	1.131	0.062	1.152
50	0.059	1.147	0.058	1.145	0.062	1.153	0.094	1.220	0.057	1.142	0.055	1.138	0.051	1.130	0.035	1.098
55	0.057	1.143	0.046	1.121	0.063	1.154	0.075	1.180					0.051	1.130	0.065	1.158

4. Discussion

Dredging is an expensive process and hundreds of millions of dollars are likely spent every year unnecessarily dredging fluid mud. This study investigates RESDIPS as a tool for distinguishing between fluid mud and hard bottoms. The investigation includes analyzing the effectiveness of processing techniques through modeling, applying theory and methods in a field test, and evaluating the quality of the results.

The finite element model is a useful tool for generating synthetic returns containing scatter. The results followed the theory of scattering in terms of the relative size between the inhomogeneities and the source wavelength. Transmission results lend credit to the effectiveness of the perturbations in the generation of scatter in all directions. The amount of scatter peaked in the 10 cm model, as expected due to the 12 kHz source. The results from each of the block sizes at 50 percent perturbation contained some residual scatter likely due to the large fluctuations in individual RCs which sometimes exceeded 0.7, seen in Figure 13. The field analogs of these conditions would be composed of hard rock and air bubbles. Rocks and bubbles can be found in unconsolidated sediment, but large volumes of large perturbations are unlikely. Furthermore, the sediment would likely need to be consolidated to support large dense objects or air bubbles. In summation, stacking is a fairly robust method and provides fair results even in high scatter environments.

The Lake Lavon field trial produced consistent results similar to those achieved in the model study over each of the four lines after stacking. The survey data appears to contain a small amount of scatter and fair SNR, similar to levels seen for models with 4 cm inhomogeneities and 25 % perturbation. A better starting SNR allows the stacking

process to produce accurate RCs after only a few stacks. The densities that are estimated appear reasonable and suggest a fluid mud with a fairly high water content. Overall, the acoustic results are promising and after more testing RESDIPS may be a valuable tool for supporting dredging operations.

The density measured in the core does not match well with the estimated acoustic densities. This mismatch may be due to the difference between the materials sampled. The fluid mud density increases with depth. The acoustic survey records the impedance contrast at the very top of the sedimentary layer where the fluid mud has the lowest density. Therefore, average core measurements from the first 12 cm of sediment should result in a higher density. It is also likely that some of the lowest density material at the water-fluid mud interface was lost during coring and not represented in the retained core sample. Hence, the densities determined from the core samples should be considered an upper bound of the in situ densities at the water-fluid mud interface.

4.1. Limitations

The model is simple and served its purpose of generating synthetic waves. However, the model's sedimentary blocks are on an identical grid for each model. The grid structure of the sediment creates perturbations that occur at the same location in the model. Thus, they produce scatter that travels the same distance, which is not truly random. Sediment realistically contains randomly located perturbations with various object dimensions within a given volume. Although this is a limitation of the model study, this is not a limitation of the finite element model.

The field method provided adequate results for the water depth surveyed. However, the instrumentation is limited by the recovery of the bottom return at greater

distances from the water bottom. The Lake Lavon survey contains reflected waves that are 600 times smaller than the direct arrival. If the array is towed at a greater distance above the water bottom, the reflected wave would not be visible. At greater distances from the water bottom the instrumentation would likely need to be modified to increase the distance between the source and receiver and increase the sensitivity of the receiver. The current processing method requires manual extraction of the direct arrival and reflected waves. This prohibits real time feedback. A commercial application of the method would require an automated extraction algorithm, control by user-selected search gates, similar to automatic bottom identification on modern fathometers.

There are also limitations in the extent to which density can be estimated from the vertical reflection coefficient. The method to estimate density assumes that the correlation in Figure 2 is fairly robust and remains true over all fluid mud. However, this assumes that all fluid mud velocities are equal to the sediment used to generate the empirical correlation. Therefore, new empirical correlations may be required in different regions. The extent to which different calibrations may be required would lessen the practicality of the method.

4.2. Future Work

The model results proved useful for investigating scatter. Although, the grid style sedimentary layer may have not produced scatter that is truly random. A realistic sedimentary matrix should be investigated to see if similar stacking results are found. The results from a matrix containing multiple perturbation sizes at random locations could also yield more applicable results for the field study.

The field results presented are promising, but additional surveys are needed to determine if this method is robust enough for commercial applications. Before an additional survey is performed, a number of improvements should be made and tested during data acquisition. It would be beneficial to test a range of frequencies in future field surveys to determine whether a higher frequency could produce adequate results. A variety of sampling methods should be tested to recover the top layer of the fluid mud for analysis. A density measurement from the top most layer is required to properly evaluate the accuracy of RESDIPS' results. To make the method commercially applicable, the processing scripts should be automated further to extract returns and estimate densities in real time. Furthermore, integrating a global positioning system (GPS) would allow maps to be generated automatically with areas labeled based on estimated densities, which would be useful for a dredging proposal.

4.3. Concluding Remarks

The modeling proves stacking is an effective method to increase the reflected signal to scattered noise ratio. However, under extreme conditions with large perturbations, stacking was unable to continually reduce the noise and stacks occasionally contained errors up to eight percent. However, the large perturbations modeled are likely unrealistic. This is supported by the Lake Lavon data where stacking consistently produced precise results. Conversely, both the model data and Lake Lavon data indicate that individual RCs are unable to produce reliable results in the presence of scatter. This confirms stacking is required to produce repeatable accurate results. Additionally, the unreliable trace by trace RCs may be a concern for higher frequency bottom typing methods such as Roxann. Lastly, the proposed acoustic method estimated reasonable

sediment densities that require further ground truthing. Stacking worked very well with the Lake Lavon test data, and the estimated densities all indicated a presence of low density mud, which is commonly found in the area.

References

Anderson, J. T., D. V. Holliday, R. Kloser, D. G. Reid, and Y. Simard (2008), Acoustic seabed classification: current practice and future directions, *ICES J. Mar. Sci. J. Cons.*, *65*(6), 1004–1011, doi:10.1093/icesjms/fsn061.

Bartholomä, A. (2006), Acoustic bottom detection and seabed classification in the German Bight, southern North Sea, *Geo-Mar. Lett.*, *26*(3), 177–184, doi:10.1007/s00367-006-0030-6.

Biffard, B. R. (2011), Seabed Remote Sensing by Single-Beam Echosounder: Models, Methods and Applications, Ph.D., University of Victoria (Canada), Canada.

Blomqvist, S. (1985), Reliability of core sampling of soft bottom sediment—an in situ study, *Sedimentology*, *32*(4), 605–612, doi:10.1111/j.1365-3091.1985.tb00474.x.

Chapman, C. (2004), *Fundamentals of Seismic Wave Propagation*, Cambridge University Press.

Gauss, R. C. (2010), The interplay of acoustic signals with boundary and volume scattering phenomena: An overview., *J. Acoust. Soc. Am.*, *128*(4), 2462–2462, doi:10.1121/1.3508819.

Greene, H. G., B. J. Todd, and Geological Association of Canada (2007), *Mapping the seafloor for habitat characterization*, Geological Association of Canada special paper ;47, Geological Association of Canada, St. John's, N.L.

Hall, C. L. (2014), A model of fluid mud transport, Ph.D., Mississippi State University, United States -- Mississippi.

Hamilton, L. (2001), Acoustic Seabed Classification Systems, *DSTO Aeronaut. Marit. Res. Lab.*

Jones, C. (2001), Sediment Sampling Guide and Methodologies,

Jones, C. D. (1999), High-frequency acoustic volume scattering from biologically active marine sediments, Ph.D., University of Washington, United States -- Washington.

Kamphuis, J., J. Verwilligen, R. Meinsma, and others (2013), Fluid mud and determining nautical depth, *Hydro Int.*, 23.

Kloser, R. J., N. J. Bax, T. Ryan, A. Williams, and B. A. Barker (2001), Remote sensing of seabed types in the Australian South East Fishery; development and application of normal incident acoustic techniques and associated "ground truthing," *Mar. Freshw. Res.*, *52*(4), 475–489.

LeBlanc, L. R., S. G. Schock, D. L. DeBruin, M. Jenkins, and L. Munro (1995), High-resolution sonar volume scattering measurements in marine sediments, *J. Acoust. Soc. Am.*, *97*(5), 2979–2986, doi:10.1121/1.411861.

Lo, T., and P. L. Inderwiesen (1994), *Fundamentals of Seismic Tomography*, SEG Books.

Luccio, M. (2014), Survey. Dredge. Repeat: Keeping the Columbia River Navigable, *xyHt*. Available from: http://www.xyht.com/hydromarine/survey-dredge-repeat-keeping-columbia-river-navigable/ (Accessed 12 October 2015)

McAnally, W. H., A. Teeter, D. Schoellhamer, C. Friedrichs, D. Hamilton, E. Hayter, P. Shrestha, H. Rodriguez, A. Sheremet, and R. Kirby (2007), Management of Fluid Mud in Estuaries, Bays, and Lakes. II: Measurement, Modeling, and Management, *J. Hydraul. Eng.*, *133*(1), 23–38, doi:10.1061/(ASCE)0733-9429(2007)133:1(23).

Moini, S., and J. Gazdag (1989), Use of frequency domain analysis for signal-to-noise ratio enhancement in stacking, in *, 1989 International Conference on Acoustics, Speech, and Signal Processing, 1989. ICASSP-89*, pp. 1583–1585 vol.3.

Schiagintweit, G. E. O. (1993), Real-time acoustic bottom classification for hydrography a field evaluation of RoxAnn, in *OCEANS '93. Engineering in Harmony with Ocean. Proceedings*, p. III/214–III/219 vol.3.

Smith, S. J., and C. T. Friedrichs (2011), Size and settling velocities of cohesive flocs and suspended sediment aggregates in a trailing suction hopper dredge plume, *Cont. Shelf Res.*, *31*(10, Supplement), S50–S63, doi:10.1016/j.csr.2010.04.002.

Solis, R. (2013), *Volumetric and Sedimentation Survey of LAVON LAKE June - July 2011 Survey*, Lavon Lake.

Soukup, D. J., and R. I. Odom (2009), Seismo-acoustic modal scattering by volume heterogeneities in shallow water sediments., *J. Acoust. Soc. Am.*, *126*(4), 2159–2159, doi:10.1121/1.3248392.

Toth, T., R. Vida, F. Horvath, and P. Simpkin (1997), Shallow-water single and multichannel seismic profiling in a riverine environment, *Lead. Edge*, *16*(11), 1691–1695.

Verna, T. (2013), *An Overview of USACE Dredging Operations*.

Welp, T. (2010), Fluid Mud/Residuals and Surveying,

CHAPTER THREE

Conclusions

This study confirms stacking as a viable method to reasonably remove scatter and receiver specular reflections in typical field environments. In addition, the Lake Lavon test demonstrates the effectiveness of a normal incidence acoustic survey as a tool for estimating densities. Future work building on this study could include other test locations to ensure the method is robust over various environments. Furthermore, the development of automated processing methods and an integrated GPS would be required for commercial applications.